iScience

CellPress
OPEN ACCESS

Article

When function is biological: Discerning how silver nanoparticle structure dictates antimicrobial activity

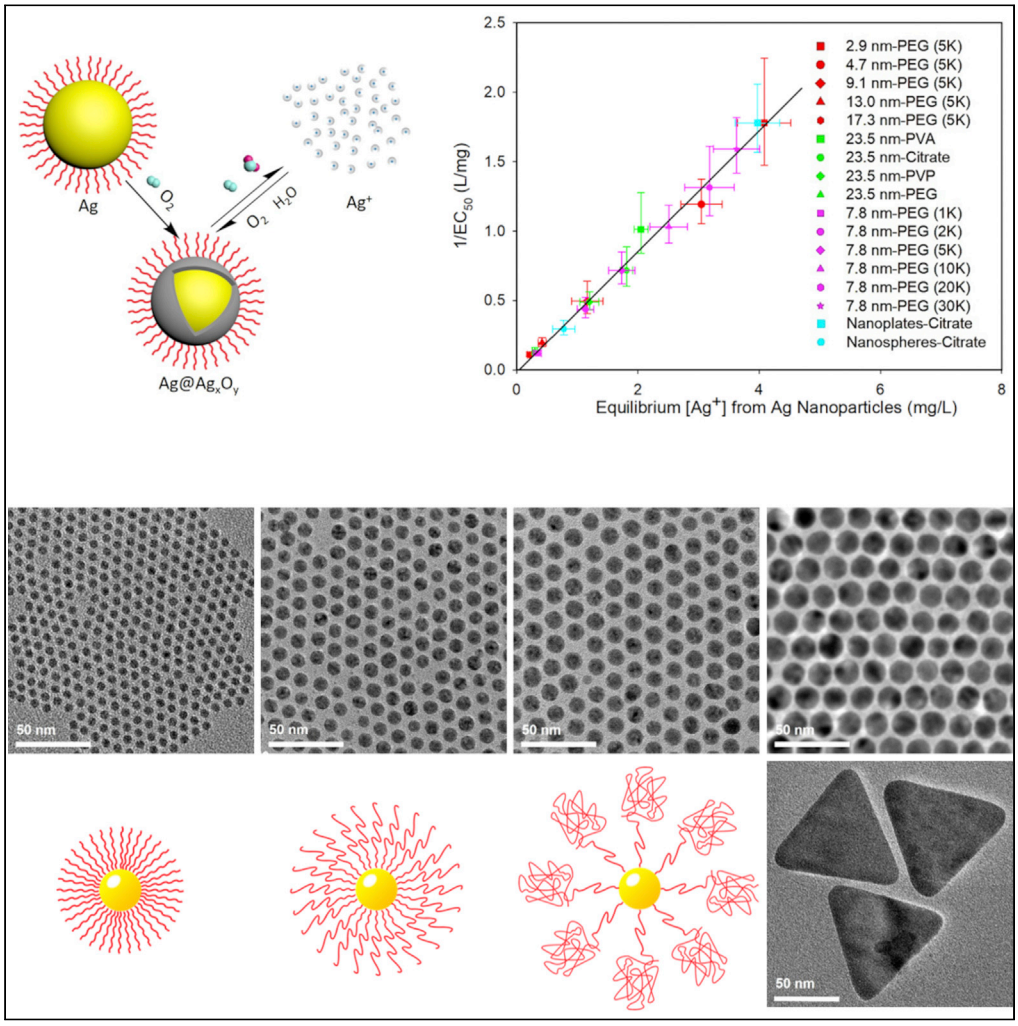

Qingbo Zhang, Yue Hu, Caitlin M. Masterson, ..., Hema L. Puppala, George Bennett, Vicki L. Colvin

colvin@brown.edu

Highlights

The oxidative dissolution of silver nanoparticles is an equilibrium process

Dissolution rate and extent depend on nanoparticle shape, size, and surface coating

The concentration of dissolved silver determines their antimicrobial efficacy

Zhang et al., iScience *25*, 104475
July 15, 2022
https://doi.org/10.1016/j.isci.2022.104475

iScience

CellPress
OPEN ACCESS

Article

When function is biological: Discerning how silver nanoparticle structure dictates antimicrobial activity

Qingbo Zhang,[1] Yue Hu,[1] Caitlin M. Masterson,[1] Wonhee Jang,[2] Zhen Xiao,[1] Arash Bohloul,[2] Daniel Garcia-Rojas,[2] Hema L. Puppala,[2] George Bennett,[3] and Vicki L. Colvin[1,4,*]

SUMMARY

Silver nanomaterials have potent antibacterial properties that are the foundation for their wide commercial use as well as for concerns about their unintended environmental impact. The nanoparticles themselves are relatively biologically inert but they can undergo oxidative dissolution yielding toxic silver ions. A quantitative relationship between silver material structure and dissolution, and thus antimicrobial activity, has yet to be established. Here, this dissolution process and associated biological activity is characterized using uniform nanoparticles with variable dimension, shape, and surface chemistry. From this, a phenomenological model emerges that quantitatively relates material structure to both silver dissolution and microbial toxicity. Shape has the most profound influence on antibacterial activity, and surprisingly, surface coatings the least. These results illustrate how material structure may be optimized for antimicrobial properties and suggest strategies for minimizing silver nanoparticle effects on microbes.

INTRODUCTION

The antibacterial properties of silver have been recognized for thousands of years (Chernousova and Epple, 2013). Silver vessels were prized for their ability to prevent spoilage of dairy products, and silver ointments were used by Greeks to prevent wound infections (Alexander, 2009). Today, numerous commercial products integrate silver, now in a more efficient nanoparticle form, for many of the same purposes (Emilio et al., 2015; Le Ouay and Stellacci, 2015; Rizzello and Pompa, 2014). Fabrics containing silver nanoparticles are marketed for their odor-resistance (Hicks and Theis, 2017); medical equipment and bandages are coated with silver nanoparticles to limit bacterial growth (Liu et al., 2017); and silver nanoparticle-laden paints, toys, and countertops promise to provide lasting antimicrobial properties (Emilio et al., 2015; Kumar et al., 2008). As a result, the annual global production of silver nanoparticles now exceeds 600 metric tons and much of this is released into ecosystems through solid waste and wastewater (Calderón-Jiménez et al., 2017; Hicks and Temizel-Sekeryan, 2019; Mitrano et al., 2014; Pourzahedi et al., 2017). This unregulated exposure is a growing concern as silver nanoparticles can impact naturally occurring microbes, aquatic ecosystems, and possibly human health (Colvin, 2003; Hansen and Baun, 2012; Khaksar et al., 2019; Nowack, 2010; Nowack et al., 2011; Su et al., 2020; Tortella et al., 2020). Manipulation of silver nanoparticle toxicity can thus lead to both improved antimicrobial technology as well as strategies for minimizing unwanted environmental effects after disposal.

To control silver nanoparticle toxicity requires control over nanoparticle dissolution (Albalghiti et al., 2021; Dedman et al., 2020; Xiu et al., 2012; Yang et al., 2012). Whether the process happens in a few hours or a few days depends on such factors as pH (Axson et al., 2015; Fernando and Zhou, 2019; Molleman and Hiemstra, 2017; Peretyazhko et al., 2014; Pokhrel et al., 2014), dissolved oxygen (Liu and Hurt, 2010; Xiu et al., 2012), ambient light (Li et al., 2013; Mittelman et al., 2015; Rong et al., 2019; Yuan et al., 2020), and the concentration of species such as sulfide and natural organic matter (Axson et al., 2015; Boehmler et al., 2020; Chambers et al., 2014; Garg et al., 2016; Gunsolus et al., 2015; Ho et al., 2011; Kittler et al., 2010; Levard et al., 2011, 2013; Li et al., 2020; Lu et al., 2016; Peng et al., 2019; Peretyazhko et al., 2014; Pokhrel et al., 2013, 2014; Yang et al., 2021). Silver ions are toxic to bacteria because they can bind to many proteins and phospholipids thereby disrupting their functions. When these ions are released by particle dissolution, they become responsible for most, if not all, of the antimicrobial activity of all types of silver

[1]Department of Chemistry and School of Engineering, Brown University, Providence RI 02912, USA

[2]Department of Chemistry, Rice University, Houston, TX 77005, USA

[3]Department of Biosciences, Rice University, Houston, TX 77005, USA

[4]Lead contact

*Correspondence: colvin@brown.edu

https://doi.org/10.1016/j.isci.2022.104475

nanomaterials (Beer et al., 2012; De Matteis et al., 2015; Xiu et al., 2012; Yang et al., 2012). When particle dissolution is made impossible, for example by the removal of all oxygen, no toxicity is observed (Xiu et al., 2012). Conversely, if nanoparticle dissolution is promoted through acidification, then antimicrobial activity can be substantially increased (Xiu et al., 2012). Manipulating the dissolution of silver nanoparticles by altering the aqueous solution, however, can be a difficult prospect to manage over the entire lifecycle of the nanoparticle.

Material structure, such as nanoparticle size and shape, should also play a significant role in silver nanoparticle dissolution and by extension antimicrobial activity (Axson et al., 2015; Feng et al., 2019; Graf et al., 2018; Long et al., 2017; Ma et al., 2012). Commercial silver nanoparticles are composed of a core of zero-valent silver metal with a surface silver oxide with diverse dimensions, shape, and surface coatings (Ma et al., 2012; Molleman and Hiemstra, 2017; Xiu et al., 2012). Qualitatively smaller nanoparticles are more toxic to bacteria on a per-mass basis and they are also likely to dissolve faster than larger particles (Axson et al., 2015; Ho et al., 2011; Molleman and Hiemstra, 2017; Peretyazhko et al., 2014; Zhang et al., 2011b). The trend follows an inverse dimension dependence, though the absolute dissolved silver concentrations are far lower than that predicted from a strict application of the Ostwald-Freundlich relationship (Liu and Hurt, 2010; Ma et al., 2012). Particle surface coating can also influence the dissolution process and toxicity to microbes and other organisms, but these observations are confounded by simultaneous nanoparticle aggregation processes that obscure trends related solely to surface functionalization (Axson et al., 2015; Fernando and Zhou, 2019; Li et al., 2013; Liu et al., 2018).

An empirical structure-activity relationship (SAR) is the next logical step in the study of silver nanoparticles. The ideal SAR would take as input the structural features of a silver nanoparticle, such as its dimensions, and predict silver dissolution as well as antimicrobial activity. One challenge in developing such data is the particles themselves. The most popular methods for forming silver nanoparticles yield materials whose dimensions, shapes, and surface chemistries are not independently controlled (Abbasi et al., 2016; Wei et al., 2015). This limits the precision of activity-structure correlations, as can the polydispersity of silver nanoparticles made from these conventional routes (Abbasi et al., 2016; Wei et al., 2015). Equally important inputs for a SAR are numerical parameters that characterize the solubility and antimicrobial activity of a sample. The dynamics of nanoparticle dissolution have been described using standard kinetic models thus providing a starting point for parameterizing this important chemical process (Ho et al., 2011; Lee et al., 2012; Liu and Hurt, 2010; Peretyazhko et al., 2014; Zhang et al., 2011b). Alternatively, the equilibrium between silver nanoparticles and silver ions may be more relevant to antimicrobial activity. Molleman et al. found a thermodynamic model can be successful in predicting steady-state silver ion concentrations providing another framework for a structure-activity relationship (Molleman and Hiemstra, 2017).

Here, we use experimental studies of model silver nanoparticles to define the relationships between silver nanoparticle structure, silver dissolution, and antimicrobial activity. Several synthetic methodologies were developed or modified to generate a large library of materials with independently tuned diameters, shapes, and surface chemistries. These nanoparticle libraries enable us to disentangle the influence of each parameter on their dissolution properties, unambiguously establishing the relationship between structural parameters and dissolution behavior. We analyzed the kinetics of silver nanoparticle dissolution, and the equilibrium behavior, using standard frameworks to extract numerical parameters to compare to structural features. The antimicrobial activity of these same samples was assessed as well. Taken together, these data provide a quantitative relationship between nanoparticle structure, dissolution rate, dissolution extent, and finally antimicrobial behavior. These results will shape more rational design of highly effective silver antimicrobials and provide a means for limiting their unintended environmental impact.

RESULTS & DISCUSSION

Silver nanoparticle libraries

Our approach to evaluating how material features influence the biological properties of silver nanoparticles relies on uniform silver nanocrystals (Figure 1). We term this large set of samples a "library" and have designed their dimensions, shapes, and surface coatings to encompass the wide range of structures used commercially. Studies of nanoscale silver derived from everyday products reveal polydisperse materials with a variety of shapes and surface coatings (Cascio et al., 2015; Rogers et al., 2018; Tulve et al., 2015). A comprehensive study of household objects, including items such as plush toys and bandages, identified nanoparticle silver that was generally spherical, with dimensions ranging from about 3 to 75 nm

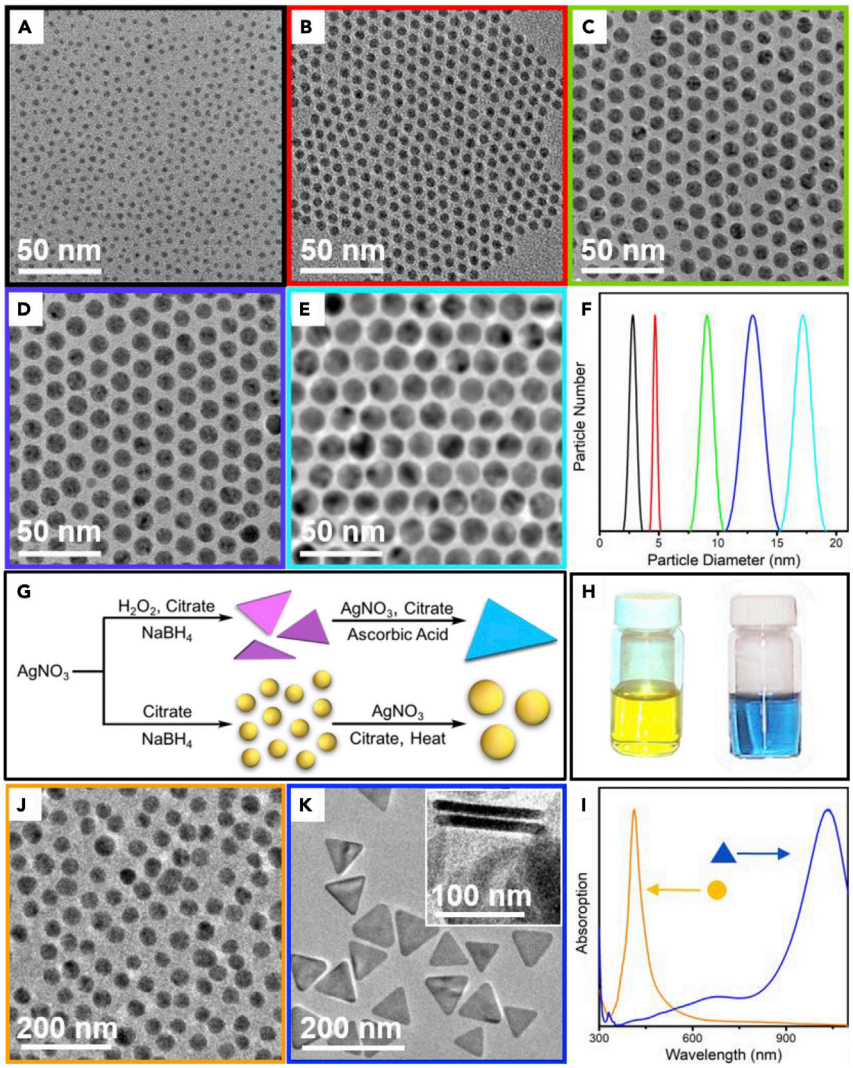

Figure 1. Silver nanoparticles with different sizes and shapes

(A–E) TEM micrographs of silver nanoparticles of 2.9 ± 0.3 nm, 4.7 ± 0.2 nm, 9.1 ± 0.5 nm, 13.0 ± 0.6 nm, and 17.3 ± 1.0 nm, respectively.

(F) Size distribution of silver nanoparticles with different diameters corresponding to the different panels. The plots are the Gaussian fits to the histograms of nanoparticle diameters found by counting over 1,500 particles in TEM micrographs.

(G) Schematic illustration of the procedure to synthesize silver nanoplates and nanospheres with identical surface coating and similar volume. The silver nanoplates and nanospheres were prepared using a two-step seeded growth method, which allows independent control of particle shape and size; (H) Photographs of aqueous solutions of silver nanospheres and nanoplates.

(I) Absorption spectra of silver nanospheres and nanoplates that were scaled to an optical density of one.

(J) TEM micrograph of silver nanospheres showing the diameter of 45.4 ± 5.4 nm.

(K) TEM micrograph of silver nanoplates showing the side length of 109 ± 11 nm. Nanoplates standing vertically upon their lateral faces (inset of (K)) showing the thickness of 9.7 ± 1.3 nm. The volumes of nanoplates and nanospheres are 49,901 nm^3 and 48,972 nm^3, respectively. See also Figures S1–S3.

(Tulve et al., 2015). Others have observed different shapes of silver particles in consumer products, including for example silver plates in spray disinfectants. Nanoscale silver used in products generally forms through the reduction of silver salts in water; a variety of polymers or surfactants are often applied to promote integration into the various product types (Abbasi et al., 2016; Wei et al., 2015). We include silver nanoparticles derived from these reactions in our library, but also examine more uniform silver nanoparticles phase transferred into water after their initial formation in organic solvents. As will be demonstrated,

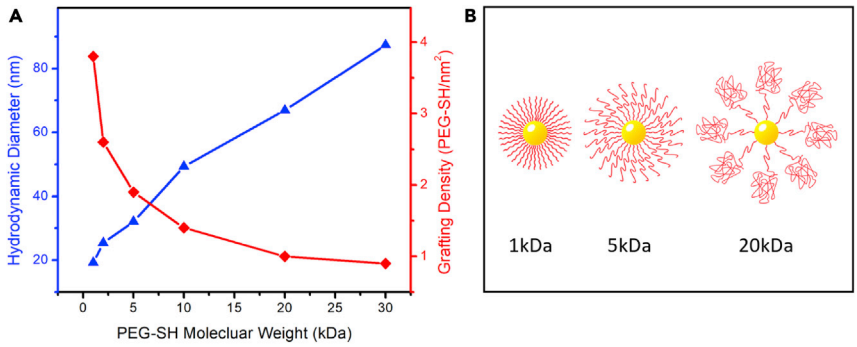

Figure 2. Silver nanoparticles coated with poly(ethylene glycol) thiol (PEG-SH) of different molecular weights

(A) Hydrodynamic diameters and grafting densities of silver nanoparticles as a function of the molecular weight of the polymer coating.

(B) The schematic illustration of silver nanoparticles coated with PEG-SH of different length showing that change of surface conformation from a linear brush to mushroom with the increase of PEG-SH chain length. Silver nanoparticles coated with PEG-SH of 1,000, 2,000, 5,000, 10,000, 20,000, and 30,000 Da were prepared through ligand exchange from the same batch of silver nanoparticles. The initial silver nanoparticles, which were synthesized through organic reaction, were originally coated with oleic acid and have a diameter of 7.8 ± 0.6 nm. See also Figures S4 and S5.

the synthetic process of nanoparticle formation has apparently no observable effect on the dissolution behavior and related antimicrobial properties.

Figure 1 illustrates the wide range of silver nanoparticles that can be generated through an adaptation of both aqueous phase and organic phase synthetic routes; most critical for our work is the ability to disentangle control of dimension from control of surface. The physical dimension of a nanoparticle is among the most important variables to vary in any study of nanoscale properties; here, the rapid thermal decomposition of silver salts forms silver nanoparticles whose dimensions can be tuned by varying the silver salt concentration, reductant strength, and capping agent. This approach allows for the generation of extremely small nanocrystals ($d < 3$ nm) as well as larger materials ($d > 30$ nm) thereby spanning the possible range of commercially relevant sizes. The high-dimensional uniformity of these materials ($\sigma < 10\%$) allows us to quantitatively evaluate size-dependent trends (Figures 1A–1F and S1). X-ray diffraction and electron diffraction identified an FCC crystal structure with unit cell dimensions equal to that observed in bulk silver; this is in good agreement with the existing literature which finds only minimal departures from single crystal unit cell dimensions in nanoparticles over 6 nm in diameter (Figure S2) (Ma et al., 2012). These silver nanoparticle samples appeared brown in water and absorption spectroscopy revealed a plasmon resonance as expected for these sizes of silver nanoparticles (Figure S3) (Zhang et al., 2009). Silver nanoplates and nanospheres with similar volume were generated from these reactions by including an oxidizing agent in the reaction (Figure 1G); the absorption spectra and digital photographs of aqueous solutions of the as-synthesized nanoplates and nanospheres show distinct colors because of their different shapes (Figures 1H and 1I) (Jin et al., 2003; Zhang et al., 2009). We chose these two nanoparticle shapes since we expect nanoplates with sharp corners and edges will show very different dissolution equilibrium and kinetics than nanospheres. The successful shape control and narrow size distribution are confirmed by the TEM micrographs of the silver nanoparticles (Figures 1J and 1K).

In addition to varying dimensions of the silver nanoparticle, we also altered the surface coating of silver nanoparticles that were otherwise equivalent in dimensions and shape. Because silver nanoparticles were formed first in non-polar media, and phase transferred into water afterward, it was possible to use identical nanoparticles and simply vary the surface capping agent. We note that such comparisons were impossible for particles formed directly in water as size control under these circumstances is intimately linked to the nature of the surface capping agent (Abbasi et al., 2016). For this surface-dependent study, we used a silver nanoparticle diameter of 7.8 ± 0.6 nm (Figure S4) and relied on the addition of sulfur-containing and hydrophilic surface polymers. What resulted is a series of samples coated with polyethylene glycol (PEG-SH) with varying chain lengths from 1,000 Da (23 units) to 30,000 Da (682 units). As expected, the hydrodynamic diameter of PEGylated silver nanoparticles increased with longer chain lengths (Figure 2A); however, the increase in the dimensions is not linear with chain length. For example, the nanoparticle with the shortest chain has a hydrodynamic diameter (H_d) of roughly 20 nm, while the material

coated with the longest chain is only four times larger in diameter. Longer chains are known to adopt more of a mushroom-like structure at nanoparticle interfaces, while shorter chains often pack effectively in dense brushes (Krueger et al., 2007). An important result here is that as a result of these conformational changes the longer chain PEG-SH has a much lower grafting density than the shorter chain PEG-SH (Figure 2B). For the shortest polymer coatings, there are more than 726 chains/particle while for the longest there are only 153 chains/particle. This translates into fewer silver-sulfur bonds for the materials coated with the highest molecular weight polymer.

To complete our silver nanoparticle library, we evaluated other surface coatings relevant to silver nanoparticle applications. For this work, we formed the initial silver nanoparticles in a conventional reaction that reduces silver salts in water in the presence of citrate; the resulting 23.5 nm diameter particles (Figure S5A) are generated with citrate as-made and are quite monodisperse compared to other examples from the literature (Li et al., 2013; Ma et al., 2012). This was achieved by increasing the reactive silver concentration to its maximum level so that diffusion-limited growth will dominate. Such a strategy precludes dimensional control but does yield a highly uniform nanoparticle at least at one size (Park et al., 2007). To replace the citrate, we mixed the suspensions with polymers such as polyvinylpyrrolidone (PVP), poly(vinyl alcohol) (PVA), and as a comparison for the materials derived in organic media, PEG-SH. Ligand exchange reactions were confirmed via spectroscopic methods and are shown in Figure S5B.

Oxidative dissolution of silver nanoparticles

Figure 3 shows that when silver nanoparticles are added to pure water under ambient conditions, they partially dissolve yielding an unchanging equilibrium concentration of soluble silver ions after several days. This behavior is observed for the entire library of nanoparticles shown in Figures 1 and 2 and S5 though important differences exist in this behavior depending on material structure (Figures 3C–3F). After only a few hours, the concentration of soluble silver is governed by kinetic considerations while at later times the concentration stabilizes as equilibrium is reached. The observation of a plateau in the dissolved silver concentration, even while there are still nanoparticles present, is the hallmark of a reaction equilibrium: the particles stop dissolving because the equilibrium concentration of soluble silver is reached. To illustrate this behavior, 23.5 nm diameter silver nanoparticles were isolated from an equilibrated solution of silver ions after nine days and redispersed in pure water. Their dissolution continues as expected as the slightly smaller nanoparticles dissolve to reach a new equilibrium level of dissolved silver (Figure 3A).

There is broad consensus that silver nanoparticles in water undergo oxidative dissolution releasing silver ions, referred to here as soluble ionic silver described by the following reaction (Liu and Hurt, 2010):

$$4\mathrm{AgNP(s)} + \mathrm{O_2(aq)} + 4\mathrm{H^+(aq)} \rightleftharpoons 4\mathrm{Ag^+(aq)} + 2\mathrm{H_2O} \qquad \text{(Equation 1)}$$

While we refer to silver nanoparticles in the above expression as AgNP(s), we note that it is the native silver oxide surface of these particles that is the reactant (Figure S6). Qualitatively, this reaction captures many aspects of silver dissolution. For example, silver nanoparticles in an anaerobic environment do not dissolve and the reaction extent increases with a decrease in pH (Molleman and Hiemstra, 2017; Xiu et al., 2012). Quantitatively, however, this chemical equilibrium has not yielded much value in terms of describing silver dissolution. At issue is whether the silver nanoparticles participate as macroscopic solids or as molecular reactants in the process. The concentration of solids in chemical equilibrium are, to the first approximation, set to one as the available bulk phase is thought to vastly exceed the concentration of any soluble product. Here, such a treatment assumes that the probability of a silver ion encountering a nanoparticle surface depends on the silver ion concentration and not the nanoparticle concentration. Liu et al. made this assumption and then used thermodynamic data about bulk silver and silver oxides to predict soluble silver ion concentrations several orders of magnitude higher than those observed experimentally (Liu and Hurt, 2010). Our own data, in agreement with one prior observation, reveal the nanoparticle concentration does influence the amount of equilibrium soluble ionic silver (Figure S7) below particle concentrations of 10 ppm (Molleman and Hiemstra, 2017). When applying silver nanoparticles in antimicrobial applications, particle concentrations may exceed 10 ppm and a description of silver ion release may be independent of nanoparticle load; conversely, in environmental applications, silver nanoparticle concentrations will be much more dilute and any model for silver ion release will require determination of local silver nanoparticle concentration.

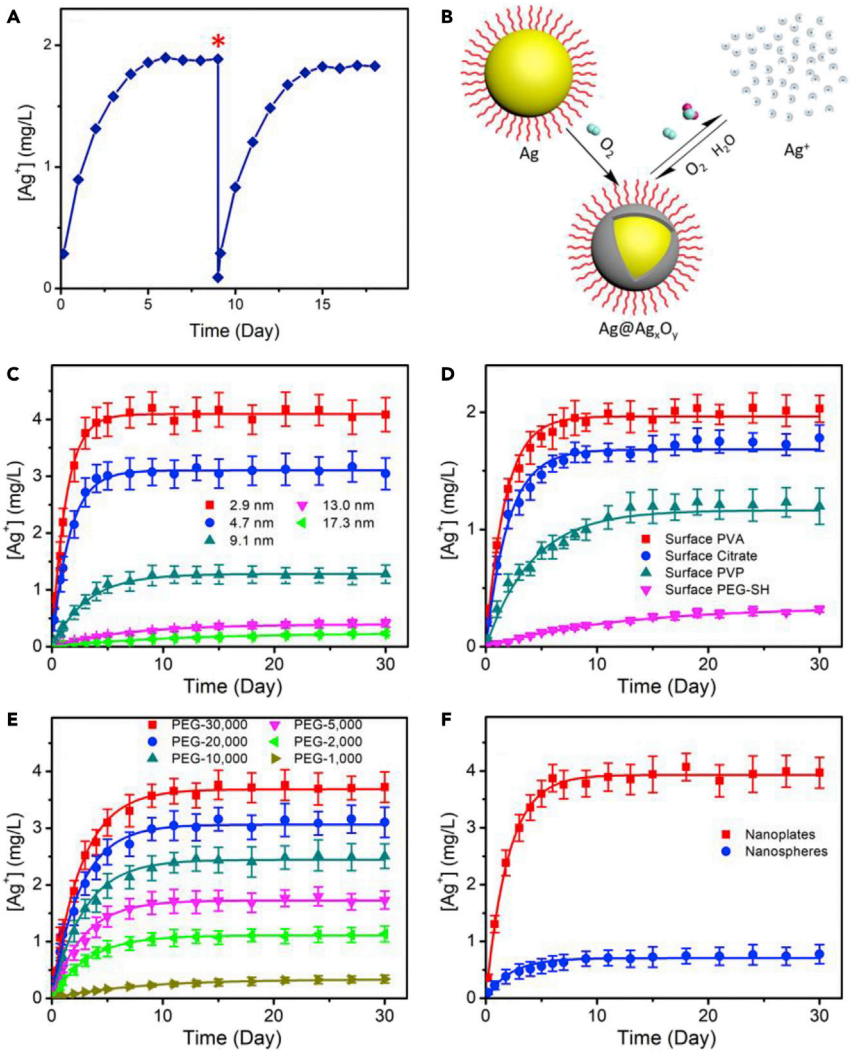

Figure 3. Dissolution of silver nanoparticles

(A) Silver nanoparticle dissolution is an equilibrium process. The silver nanoparticles (d = 23.5 ± 2.6 nm) were coated with poly(vinyl alcohol) (PVA, 9,000–10,000) for these experiments. The concentration of silver ions in the solution increases with time due to the oxidative dissolution of silver nanoparticles and becomes constant after a period of time (~5 days). The silver nanoparticles were isolated from the solution by centrifugal filter and redispersed in water after nine days. The dissolution restarts following similar profile until the concentration of silver ions becomes constant again. These observations show that the dissolution of silver nanoparticles is an equilibrium process. (B) Schematic illustration of oxidative dissolution of silver nanoparticles. A layer of oxidized silver will be formed once silver nanoparticles are exposed to dissolved oxygen in water. There exists an equilibrium between oxidized silver on particle surfaces and dissolved silver in solution.

(C) Dissolution properties of silver nanoparticles with different diameters. The silver nanoparticles were coated with poly(ethylene glycol) thiol (PEG-SH, 5,000). The error bars shown here, and in D-F, are the standard deviation of triplicate measurements.

(D) Dissolution properties of silver nanoparticles (23.5 ± 2.6 nm) with different surface coatings; (E) Dissolution properties of silver nanoparticles (7.8 ± 0.6 nm) coated with PEG-SH of different molecular weights.

(F) Dissolution properties of citrate-coated silver nanoparticles with different shapes. In all cases, symbols are the concentration of silver ion as measured with an ion-selective electrode; the lines represent fits to the data using the first-order reaction model described in the supplemental information. The initial concentration of silver nanoparticles is 12. mg/L for all samples. See also Figures S6–S8, and Table S1.

In the dilute limit, the probability of silver ions encountering a nanoparticle interface does depend on nanoparticle concentration yielding an equilibrium expression that explicitly includes nanoparticle concentration:

$$[Ag^+] = K_{eq}[O_2]^{\frac{1}{4}}[H^+][AgNP : SA] \quad \text{(Equation 2)}$$

Because dissolution necessarily happens at the interface of the particle, we use [AgNP:SA] to refer to the amount of nanoparticle surface area per volume of suspension (Molleman and Hiemstra, 2017). Over our broad range of silver nanoparticle structures at a relatively high starting concentration of 12 ppm total silver, we find that at equilibrium between 2% and 34% of the total silver is released as ionic silver at equilibrium (Figures 3C–3F) for these solution conditions (e.g. room temperature and ambient light). For the same mass weight of atomic silver in a suspension, smaller particles will dissolve to a greater extent than larger ones because they have more available surface area (Figure 3C). This qualitative trend has been observed in many types of silver and under different solution conditions (Ma et al., 2012; Molleman and Hiemstra, 2017; Zhang et al., 2011b). Our data are in good agreement with these prior findings across particles prepared in different ways. At a fixed atomic silver concentration of 12 ppm, the largest nanoparticles produced only 0.24 ppm of soluble silver after 7 days while the smallest ones yielded 4.1 ppm.

We then evaluated whether the general trend of more dissolution with smaller particle size can be described quantitatively: could the equilibrium silver concentrations of larger particles be predicted from the behavior of smaller particles? Figure 3C shows the relationship is well described from the dependence of the reaction on the available silver surface area (Equation 2). For nanoparticle prepared at the same "per-atom" silver concentration, Equation 2 would predict that the equilibrium silver should be proportional to the particle surface area divided by the particle number. Such a relationship is clearly observed for particles over 8 nm diameter (Figure S8).

We observe that for the very smallest silver nanoparticles the amount of silver released is less than expected from the behavior of their larger counterparts. Specifically, the measured concentration of silver ions is much smaller than predicted from a simple consideration of nanoparticle geometry. We hypothesize that at the very smallest sizes the equilibrium constant, Keq, is no longer independent of dimension due to changes in the nanoparticle structure. Molleman and Hiemstra suggested the surface layer of silver nanoparticles in aqueous solution consists of interfacial oxidized silver distinct from the bulk phase (Molleman and Hiemstra, 2015). Additionally, small face-center cubic metal nanoparticles may assume unique structures composed of several complete closely packed shells (Desireddy et al., 2013). In either case, the changing structures of the very smallest particles can act to stabilize the nanoparticle reactant and may account for this data. This observation has two consequences. First, given the relatively larger dimensions of commercial nanoscale silver, it should be possible to describe most of the dissolution process using simple calculations of the particle surface area. Additionally, non-equilibrium processes that seek to completely dissolve silver nanoparticles may be stymied as extremely small silver nanoparticles adopt more stable structures distinct from bulk silver.

The nanoparticle surface coating can be at least as important as particle dimension in dictating the amount of soluble silver formed at equilibrium (Figure 3D). Nanoparticles that have stronger bonds with surface coatings, and more of these bonds, will dissolve less than nanoparticles with fewer and weaker bonds to surface coatings. We found that for identical nanoparticles the chemical nature of the surface coating affected dissolution in the following sequence: PVA [poly (vinyl alcohol)] > Citrate > PVP [poly (vinyl pyrrolidone)] > PEG-SH [poly (ethylene glycol)] (Figure 3D). The strongest bond (217 kJ/mol) is between the silver and sulfur of the PEGylated particles and the weakest is the coordination of the silver to the hydroxyl groups of the poly(vinyl alcohol) coating (Lide, 2001). An additional finding is that for the same surface coating dissolution is a sensitive function of the number of bonds between the surface coating and the particle. The grafting density of PEG-SH on nanoparticle surfaces decreases with the polymer length so that there are fewer chains bound when chain lengths are longer (Figure 2A). Fewer polymers at the nanoparticle interface translate into fewer Ag-S bonds and an equilibrium more strongly shifted toward dissolution (Figure 3E).

Surface morphology can also exert a notable effect on nanoparticle dissolution in that higher surface energy shapes dissolve more rapidly than silver nanospheres (Figure 3F). We formed silver nanospheres and nanoplates with identical surface chemistry and volume and found each had different dissolution

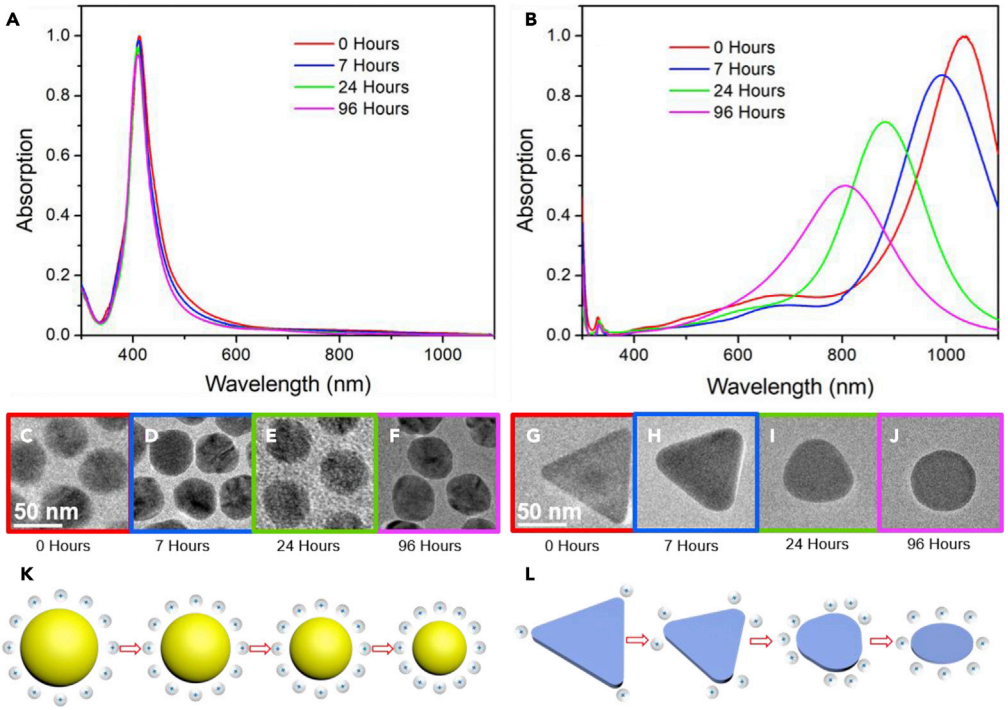

Figure 4. Dissolution process of silver nanospheres and nanoplates

(A) Absorption spectra of silver nanospheres at different stages of dissolution.

(B) Absorption spectra of silver nanoplates at different stages of dissolution.

(C–F) TEM micrographs of silver nanospheres at different stages of dissolution.

(G–J) TEM micrographs of silver nanoplates at different stages of dissolution.

(K) The schematic illustration of the dissolution process of silver nanospheres.

(L) The schematic illustration of the dissolution process of silver nanoplates. Both the spectroscopic and microscopic data illustrated how silver nanospheres dissolve uniformly and retain their shape; in converse, the sharp tips of the nanoplates are more prone to dissolution giving rise to a pronounced shape evolution as dissolution proceeds.

characteristics. High aspect ratio materials dissolve preferentially form their highest energy surface structures, here the plate tips, resulting in profound changes in particle shape; nanospheres in contrast undergo no shape changes while they dissolve (Figure 4) (Graf et al., 2018). The dissolution of silver nanoplates occurred preferentially on the lateral faces because of their higher surface energy, a consequence of their small dimensions, and high-energy crystallographic facets (100) (Jin et al., 2003; Lofton and Sigmund, 2005).

While the prior discussion focused the extent of silver dissolution at equilibrium, the speed of nanoparticle dissolution is equally important. Silver ion release can be slow and under our conditions took from several days to weeks; instead of monitoring a solution until it reached equilibrium, early dynamic studies of silver ion release might provide a more practical dissolution parameter to characterize. We found that over a wide range of particle types, shapes, and dimensions the speed of dissolution was proportional to the equilibrium silver ion concentration. Figure 5 shows that the half-life of the dissolution process is inversely proportional to the final equilibrium silver concentration: nanoparticles that dissolve to a greater extent also dissolve faster with two notable exceptions. The first are non-spherical particles. As they undergo dissolution, they also change their shape, leading to more complex equilibrium and kinetic behaviors. The second are particles with longer length polymer coatings. In these examples, particle dissolution rate is slower than expected and we speculate that diffusion of ions through the surface coatings may slow down the dissolution process. We note that in agreement with past reports our dissolution kinetics are well described by a pseudo-first order reaction rate model which treats the formation of the silver ion as the rate-limiting step (Figure 5) (Ho et al., 2011; Kittler et al., 2010; Zhang et al., 2011b). The extracted rate constants for our wide range of materials are in the range of those reported for studies of other silver nanoparticles and are reported in Table S1 (Ho et al., 2011; Kittler et al., 2010; Zhang et al., 2011b).

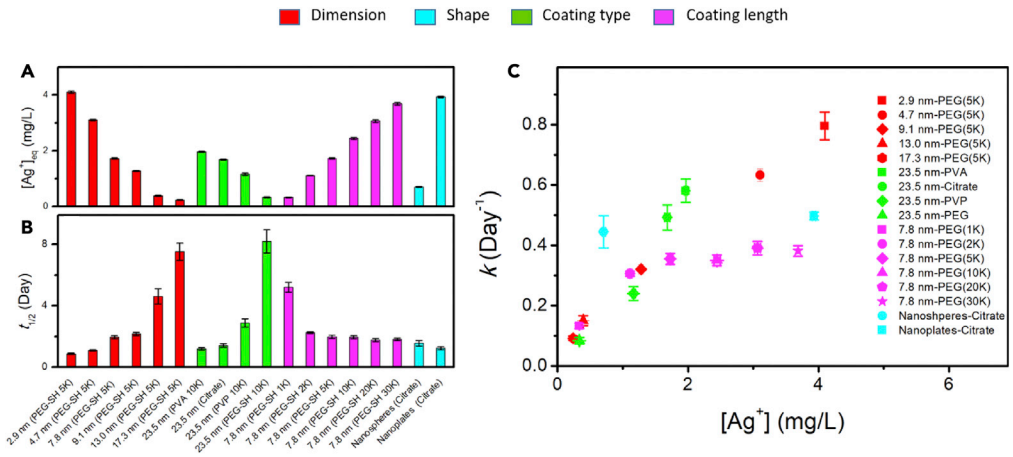

Figure 5. How nanoparticle structure affects the extent and the kinetics of particle dissolution

(A) Equilibrium concentrations of silver ions were obtained from fits to the pseudo-first order reaction rate model described in the supplemental experimental text. Error bars shown in these data are the standard deviation of fits taken from replicate time-dependent dissolution datasets.

(B) The half-lives found from the dissolution kinetics show distinctive trends with respect to the particle structure; the reaction rate constant, k, in this analysis is inversely proportional to $1/t_{1/2}$.

(C) The relationship between the reaction rate constant and equilibrium concentrations of silver ions. The data show that nanoparticles that dissolve to a greater extent also dissolve faster with two notable exceptions. The first are non-spherical particles. The second are particles with very long or dense surface coatings such as nanoparticles coated with PEG-SH larger than 10 kDa. The samples studied include poly(ethylene glycol) thiol (PEG-SH, 5,000)-coated silver nanoparticles of different diameters (2.9 $\pm$ 0.3 nm, 4.7 $\pm$ 0.2 nm, 9.1 $\pm$ 0.5 nm, 13.0 $\pm$ 0.6 nm, and 17.3 $\pm$ 1.0 nm); 23.5 $\pm$ 2.6 nm silver nanoparticles with different surface coatings (Poly(ethylene glycol) thiol, Poly(vinyl pyrrolidone), Poly(vinyl alcohol), and Citrate.); 7.8 $\pm$ 0.6 nm silver nanoparticles coated with PEG-SH of different molecular weight (1,000, 2000, 5000, 10,000, 20,000, and 30,000); citrate-coated silver nanoparticles with different shapes (nanospheres and nanoplates). The initial concentration of silver nanoparticles is 12. mg/L for all samples. See also Table S2.

Antimicrobial activity of silver nanoparticles

Ultimately, the silver nanoparticle dissolution process is important because of its role in mediating the antimicrobial activity of these materials. This property is directly proportional to the amount of soluble silver released by the nanoparticles (Figure 6). We evaluated this effect by exposing *E. coli*, a model microorganism, to various silver nanoparticles and applied a standard assay to evaluate the dose of material required to kill half of a population. This figure of merit, termed the EC_{50}, tracks closely the equilibrium and kinetic dissolution behavior described previously. Figure 6A shows that over a wide range of material types, the EC_{50} of silver nanoparticles is inversely proportional to the equilibrium concentration of soluble silver. We also investigated two particles with comparable equilibrium behavior but different dissolution kinetics, namely fast-dissolving nanoplates with edge lengths of 120 $\pm$ 14 nm (Figure S9A) and slow-dissolving nanospheres of 8.3 $\pm$ 0.7 nm (Figure S9B). The antibacterial effectiveness of each particle type over time tracked their release of soluble silver available at any given time point (Figure 6B). Thus, at short times, the silver nanoplates were more toxic than the nanospheres but when evaluated after reaching equilibrium their overall effects were similar.

The silver nanoparticle libraries evaluated here illustrate how nanoparticle structure may be used to either amplify antimicrobial properties, as may be useful in applications, or conversely minimize these same properties upon disposal. As shown in Figure 6, the best antimicrobial materials are the nanoplates which by virtue of their high surface energy dissolve quickly and yield high amounts of soluble silver (3.93 ppm). In contrast, the least biologically active nanoparticles are larger, spherical particles which have dense coatings and many silver-sulfur bonds at their interface. Equilibrium silver ion concentration remained below our detection limit for 17 nm diameter silver nanoparticles coated with polyethylene glycol; conversely, silver ion concentrations could be as high as 5 ppm for 7 nm diameter silver nanoparticles stabilized by weak coordination with citrate. Forming highly insoluble silver sulfide coatings could be a strategy for mitigating potential environmental risk after disposal, though the stability of such bonds may be poor in moderately acidic settings (Levard et al., 2011).

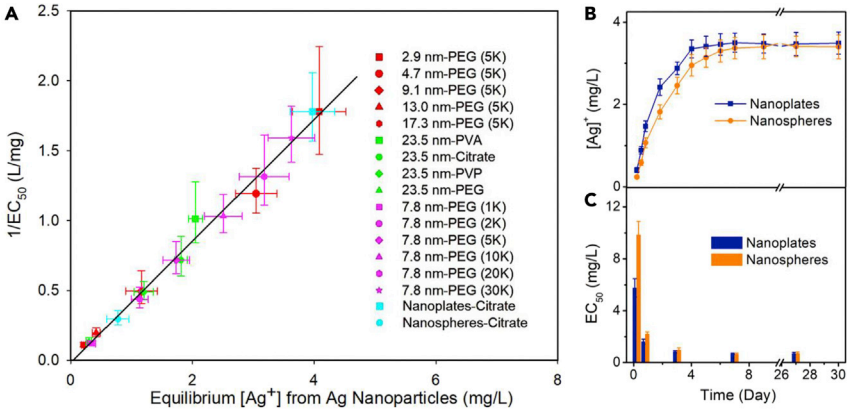

Figure 6. The antimicrobial properties of silver nanoparticles can be directly correlated to the extent of nanoparticle dissolution as measured by the equilibrium silver ion concentration

(A) For a wide range of silver nanoparticle types, the antibacterial potency of the materials is linearly proportional to the equilibrium concentrations of silver ions released. These samples include poly(ethylene glycol) thiol (PEG-SH, 5,000)-coated silver nanoparticles of different diameters (2.9 ± 0.3 nm, 4.7 ± 0.2 nm, 9.1 ± 0.5 nm, 13.0 ± 0.6 nm, and 17.3 ± 1.0 nm); 23.5 ± 2.6 nm silver nanoparticles with different surface coatings (Poly(ethylene glycol) thiol, Poly(vinyl pyrrolidone), Poly(vinyl alcohol), and Citrate.); 7.8 ± 0.6 nm silver nanoparticles coated with PEG-SH of different molecular weight (1,000, 2000, 5000, 10,000, 20,000, and 30,000); citrate-coated silver nanoparticles with different shapes (nanospheres and nanoplates). The dots represent the measured EC50 has defined in the text of the silver nanoparticles (y axis) and equilibrium concentration of silver ions released from the oxidative dissolution of silver nanoparticles (x axis). In two cases, the antimicrobial properties were measured prior to the samples achieving equilibrium and the line represents the linear fit to the measured data.

(B and C). The nanospheres were coated with Poly(ethylene glycol) thiol (PEG-SH, 30,000) and have a diameter of 8.3 nm. The nanoplates were coated with citrate and have a side length of 120 nm. Panel B and C share the same x axis for easy comparison. The antimicrobial efficiency of each particle type tracks their release of soluble silver over time. See also Figure S9.

We conclude by comparing how important silver nanoparticle material structure may be relative to the solution conditions known to affect nanoparticle dissolution. Previous reports have detailed how temperature, pH, light exposure, and the presence of organic and inorganic ligands influence this dissolution process. Figure 7 shows that in this work, through control of nanoparticle structure, the equilibrium silver ion concentration can be varied from 240 to 4000 ppb. This range of behavior is comparable to that observed for different solution conditions; ions such as chloride and sulfide as an example can significantly promote or inhibit dissolution as we would expect from the dissolution reaction (Equation 2). This analysis suggests that characterization of silver nanoparticle structure, particularly if it is high aspect ratio or stabilized through sulfur-containing coatings, is important for predicting dissolution properties. The structure-function relationships shown here illustrate how both changes in silver nanomaterial form as well as changes in the solution environment, if they can be triggered intelligently, could enable next-generation antimicrobial materials capable of releasing silver only when needed.

Conclusions

There is a need to predict how silver nanoparticle features influence their antimicrobial potency as well as environmental impact. This work systematically investigated these issues using a library of model silver nanoparticles tailored to exhibit a wide range of dimensions, shapes, and surface treatments. Measurement of the dissolved silver in nanoparticle suspensions over time revealed that dissolution is an equilibrium process: soluble silver concentrations increase over days, following pseudo-first-order reaction kinetics, until the concentration reaches a constant, equilibrium value. As expected with more surface area of silver available, such as at higher concentrations of nanoparticles, there is more dissolved silver. Likewise, for the same mass concentration of silver, smaller particles dissolve to a greater extent than larger particles in a manner predicted by their larger relative surface areas. Exceptions to these general trends are only observed at high concentrations of silver nanoparticles ([Ag] > 10 ppm) and extremely small (d < 4 nm) silver nanocrystals. Also notable is that for virtually all materials the speed of the dissolution process was proportional to its degree: nanoparticles that dissolved faster also dissolved to a greater extent.

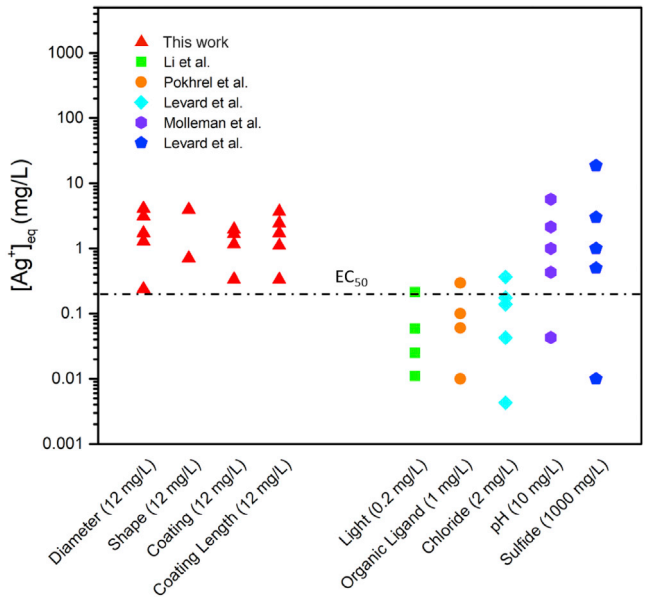

Figure 7. The effect of structural parameters and environmental conditions on the equilibrium concentration of silver ions

The red symbols on the left of the figure show the effects of the structural parameters investigated in this work on the equilibrium concentration of silver ions. The symbols on the right of the figure show the effect of environmental conditions on the equilibrium concentration of silver ions. These data were extracted from references 29, 35, 38, 43, and 44. The structural parameters, the concentration of silver, and the dissolution conditions are summarized in Table S1 and Table S2. The data show that both the structural parameters and environmental conditions have significant influence on the equilibrium concentrations of silver ions.

Antimicrobial efficacy is linearly correlated to the concentration of dissolved silver and apparently insensitive to the nanoparticle structure. These findings not only shed a great deal of light on the understanding the chemistry of silver on the nanoscale but also pave the way toward efficient and safe use of silver nanoparticles by design.

Limitations of the study

In this work, we established the quantitative relationship between silver nanoparticle dissolution and their structural parameters. All of the experiments in this work were performed in pure water at room temperature. Previous study showed that environmental conditions, such as temperature, light, and ligands in the solution, have significant influence on the dissolution rate and extent of silver nanoparticles. Further study is needed to determine the structure-activity relationship of silver nanoparticles under conditions in real applications.

STAR★METHODS

Detailed methods are provided in the online version of this paper and include the following:

- KEY RESOURCES TABLE
- RESOURCE AVAILABILITY
  - Lead contact
  - Materials availability
  - Data and code availability
- EXPERIMENTAL MODEL AND SUBJECT DETAILS
  - Bacteria
- METHOD DETAILS
  - Silver nanoparticles with different size
  - Phase transfer of silver nanoparticles
  - Silver nanoparticles with different shapes
  - Silver nanoparticles with different coatings

- Silver nanoparticles with different PEG length
- Transmission electron microscopy
- Infrared spectroscopy
- Optical spectroscopy
- Atomic emission spectroscopy
- Dynamic light scattering
- X-ray photoelectron spectroscopy
- Measurement of PEG grafting density
- Measurement of silver dissolution
- Measurement of the antibacterial activity

● QUANTIFICATION AND STATISTICAL ANALYSIS

SUPPLEMENTAL INFORMATION

Supplemental information can be found online at https://doi.org/10.1016/j.isci.2022.104475.

ACKNOWLEDGMENTS

We acknowledge the financial support from Brown University (CC13210.1091), Environmental Protection Agency (RD-834557501-0), National Science Foundation (CMMI-1057906), Center for Biological and Environmental Nanotechnology (NSF grant EEC-0647452). QZ thanks Dr. Bo Chen from Shared Equipment Authority, Rice University for his help in XPS measurement.

AUTHOR CONTRIBUTIONS

Conceptualization, Q.Z. and V.L.C.; Methodology, Q.Z. and V.L.C.; Investigation, Q.Z., Y.H., C.M.M., W.J., Z.X., A.B., D.G.R., H.L.P., G.B., and V.L.C; Writing – Original Draft, Q.Z., Y.H., C.M.M., and V.L.C; Funding Acquisition, V.L.C.; Resources, G.B. and V.L.C.; Supervision, V.L.C.

DECLARATION OF INTERESTS

The authors declare no competing interests.

Received: May 17, 2021
Revised: May 5, 2022
Accepted: May 20, 2022
Published: July 15, 2022

REFERENCES

Abbasi, E., Milani, M., Fekri Aval, S., Kouhi, M., Akbarzadeh, A., Tayefi Nasrabadi, H., Nikasa, P., Joo, S.W., Hanifehpour, Y., Nejati-Koshki, K., and Samiei, M. (2016). Silver nanoparticles: synthesis methods, bio-applications and properties. Crit. Rev. Microbiol. *42*, 173–180. https://doi.org/10.3109/1040841x.2014.912200.

Albalghiti, E., Stabryla, L.M., Gilbertson, L.M., and Zimmerman, J.B. (2021). Towards resolution of antibacterial mechanisms in metal and metal oxide nanomaterials: a meta-analysis of the influence of study design on mechanistic conclusions. Environmental Science-Nano *8*, 37–66. https://doi.org/10.1039/d0en00949k.

Alexander, J.W. (2009). History of the medical use of silver. Surg. Infect. *10*, 289–292. https://doi.org/10.1089/sur.2008.9941.

Axson, J.L., Stark, D.I., Bondy, A.L., Capracotta, S.S., Maynard, A.D., Philbert, M.A., Bergin, I.L., and Ault, A.P. (2015). Rapid kinetics of size and pH-dependent dissolution and aggregation of silver nanoparticles in simulated gastric fluid. J. Phys. Chem. C *119*, 20632–20641. https://doi.org/10.1021/acs.jpcc.5b03634.

Beer, C., Foldbjerg, R., Hayashi, Y., Sutherland, D.S., and Autrup, H. (2012). Toxicity of silver nanoparticles—nanoparticle or silver ion? Toxicol. Lett. *208*, 286–292. https://doi.org/10.1016/j.toxlet.2011.11.002.

Benoit, D.N., Zhu, H.G., Lilierose, M.H., Verm, R.A., Ali, N., Morrison, A.N., Fortner, J.D., Avendano, C., Ayendano, C., and Colvin, V.L. (2012). Measuring the grafting density of nanoparticles in solution by analytical ultracentrifugation and total organic carbon analysis. Anal. Chem. *84*, 9238–9245. https://doi.org/10.1021/ac301980a.

Boehmler, D.J., O'Dell, Z.J., Chung, C., and Riley, K.R. (2020). Bovine serum albumin enhances silver nanoparticle dissolution kinetics in a size- and concentration-dependent manner. Langmuir *36*, 1053–1061. https://doi.org/10.1021/acs.langmuir.9b03251.

Calderón-Jiménez, B., Johnson, M.E., Montoro Bustos, A.R., Murphy, K.E., Winchester, M.R., and Vega Baudrit, J.R. (2017). Silver nanoparticles: technological advances, societal impacts, and metrological challenges. Front. Chem. *5*, 6. https://doi.org/10.3389/fchem.2017.00006.

Cascio, C., Geiss, O., Franchini, F., Ojea-Jimenez, I., Rossi, F., Gilliland, D., and Calzolai, L. (2015). Detection, quantification and derivation of number size distribution of silver nanoparticles in antimicrobial consumer products. J. Anal. At. Spectrom. *30*, 1255–1265. https://doi.org/10.1039/c4ja00410h.

Chambers, B.A., Afrooz, A.R.M.N., Bae, S., Aich, N., Katz, L., Saleh, N.B., and Kirisits, M.J. (2014). Effects of chloride and ionic strength on physical morphology, dissolution, and bacterial toxicity of silver nanoparticles. Environ. Sci. Technol. *48*, 761–769. https://doi.org/10.1021/es403969x.

Chernousova, S., and Epple, M. (2013). Silver as antibacterial agent: ion, nanoparticle, and metal. Angew. Chem. Int. Ed. *52*, 1636–1653. https://doi.org/10.1002/anie.201205923.

Colvin, V.L. (2003). The potential environmental impact of engineered nanomaterials. Nat. Biotechnol. *21*, 1166–1170. https://doi.org/10.1038/nbt875.

De Matteis, V., Malvindi, M.A., Galeone, A., Brunetti, V., De Luca, E., Kote, S., Kshirsagar, P., Sabella, S., Bardi, G., and Pompa, P.P. (2015). Negligible particle-specific toxicity mechanism of silver nanoparticles: the role of Ag+ ion release in the cytosol. Nanomed. Nanotechnol. Biol. Med. *11*, 731–739. https://doi.org/10.1016/j.nano.2014.11.002.

Dedman, C.J., Newson, G.C., Davies, G.L., and Christie-Oleza, J.A. (2020). Mechanisms of silver nanoparticle toxicity on the marine cyanobacterium Prochlorococcus under environmentally-relevant conditions. Sci. Total Environ. *747*, 141229. https://doi.org/10.1016/j.scitotenv.2020.141229.

Desireddy, A., Conn, B.E., Guo, J., Yoon, B., Barnett, R.N., Monahan, B.M., Kirschbaum, K., Griffith, W.P., Whetten, R.L., Landman, U., and Bigioni, T.P. (2013). Ultrastable silver nanoparticles. Nature *501*, 399–402. https://doi.org/10.1038/nature12523.

Emilio, I., Alarcon, M.G., and Udekwu, K.I. (2015). Silver Nanoparticle Applications (Springer International Publishing).

Feng, Y.L., Wang, G.R., Chang, Y., Cheng, Y., Sun, B.B., Wang, L.M., Chen, C.Y., and Zhang, H.Y. (2019). Electron compensation effect suppressed silver ion release and contributed safety of Au@Ag core-shell nanoparticles. Nano Lett. *19*, 4478–4489. https://doi.org/10.1021/acs.nanolett.9b01293.

Fernando, I., and Zhou, Y. (2019). Impact of pH on the stability, dissolution and aggregation kinetics of silver nanoparticles. Chemosphere *216*, 297–305. https://doi.org/10.1016/j.chemosphere.2018.10.122.

Garg, S., Rong, H.Y., Miller, C.J., and Waite, T.D. (2016). Oxidative dissolution of silver nanoparticles by chlorine: implications to silver nanoparticle fate and toxicity. Environ. Sci. Technol. *50*, 3890–3896. https://doi.org/10.1021/acs.est.6b00037.

Graf, C., Nordmeyer, D., Sengstock, C., Ahlberg, S., Diendorf, J., Raabe, J., Epple, M., Köller, M., Lademann, J., Vogt, A., et al. (2018). Shape-dependent dissolution and cellular uptake of silver nanoparticles. Langmuir *34*, 1506–1519. https://doi.org/10.1021/acs.langmuir.7b03126.

Gunsolus, I.L., Mousavi, M.P.S., Hussein, K., Bühlmann, P., and Haynes, C.L. (2015). Effects of humic and fulvic acids on silver nanoparticle stability, dissolution, and toxicity. Environ. Sci. Technol. *49*, 8078–8086. https://doi.org/10.1021/acs.est.5b01496.

Hansen, S.F., and Baun, A. (2012). When enough is enough. Nat. Nanotechnol. *7*, 409–411. https://doi.org/10.1038/nnano.2012.115.

Hicks, A.L., and Temizel-Sekeryan, S. (2019). Understanding the potential environmental benefits of nanosilver enabled consumer products. NanoImpact *16*, 100183. https://doi.org/10.1016/j.impact.2019.100183.

Hicks, A.L., and Theis, T.L. (2017). A comparative life cycle assessment of commercially available household silver-enabled polyester textiles. Int. J. Life Cycle Assess. *22*, 256–265. https://doi.org/10.1007/s11367-016-1145-2.

Ho, C.M., Wong, C.K., Yau, S.K.W., Lok, C.N., and Che, C.M. (2011). Oxidative dissolution of silver nanoparticles by dioxygen: a kinetic and mechanistic study. Chemistry-an Asian Journal *6*, 2506–2511. https://doi.org/10.1002/asia.201100034.

Jin, R., Charles Cao, Y., Hao, E., Métraux, G.S., Schatz, G.C., and Mirkin, C.A. (2003). Controlling anisotropic nanoparticle growth through plasmon excitation. Nature *425*, 487–490. https://doi.org/10.1038/nature02020.

Khaksar, M., Vasileiadis, S., Sekine, R., Brunetti, G., Scheckel, K.G., Vasilev, K., Lombi, E., and Donner, E. (2019). Chemical characterisation, antibacterial activity, and (nano)silver transformation of commercial personal care products exposed to household greywater. Environmental Science-Nano *6*, 3027–3038. https://doi.org/10.1039/c9en00738e.

Kittler, S., Greulich, C., Diendorf, J., Köller, M., and Epple, M. (2010). Toxicity of silver nanoparticles increases during storage because of slow dissolution under release of silver ions. Chem. Mater. *22*, 4548–4554. https://doi.org/10.1021/cm100023p.

Krueger, K.M., Al-Somali, A.M., Mejia, M., and Colvin, V.L. (2007). The hydrodynamic size of polymer stabilized nanocrystals. Nanotechnology *18*, 475709. https://doi.org/10.1088/0957-4484/18/47/475709.

Kumar, A., Vemula, P.K., Ajayan, P.M., and John, G. (2008). Silver-nanoparticle-embedded antimicrobial paints based on vegetable oil. Nat. Mater. *7*, 236–241. https://doi.org/10.1038/nmat2099.

Le Ouay, B., and Stellacci, F. (2015). Antibacterial activity of silver nanoparticles: a surface science insight. Nano Today *10*, 339–354. https://doi.org/10.1016/j.nantod.2015.04.002.

Lee, Y.J., Kim, J., Oh, J., Bae, S., Lee, S., Hong, I.S., and Kim, S.H. (2012). Ion-release kinetics and ecotoxicity effects of silver nanoparticles. Environ. Toxicol. Chem. *31*, 155–159. https://doi.org/10.1002/etc.717.

Levard, C., Mitra, S., Yang, T., Jew, A.D., Badireddy, A.R., Lowry, G.V., and Brown, G.E. (2013). Effect of chloride on the dissolution rate of silver nanoparticles and toxicity to E. coli. Environ. Sci. Technol. *47*, 5738–5745. https://doi.org/10.1021/es400396f.

Levard, C., Reinsch, B.C., Michel, F.M., Oumahi, C., Lowry, G.V., and Brown, G.E., Jr. (2011). Sulfidation processes of PVP-coated silver nanoparticles in aqueous solution: impact on dissolution rate. Environ. Sci. Technol. *45*, 5260–5266. https://doi.org/10.1021/es2007758.

Li, N., Zhang, Q., Quinlivan, S., Goebl, J., Gan, Y., and Yin, Y. (2012). H2O2-Aided seed-mediated synthesis of silver nanoplates with improved yield and efficiency. ChemPhysChem *13*, 2526–2530. https://doi.org/10.1002/cphc.201101018.

Li, P., Peng, Q., and Li, Y. (2011). Controlled synthesis and self-assembly of highly monodisperse Ag and Ag2S nanocrystals. Chem. Eur J. *17*, 941–946. https://doi.org/10.1002/chem.201000724.

Li, P.H., Su, M., Wang, X.D., Zou, X.Y., Sun, X., Shi, J.P., and Zhang, H.W. (2020). Environmental fate and behavior of silver nanoparticles in natural estuarine systems. JEnvS *88*, 248–259. https://doi.org/10.1016/j.jes.2019.09.013.

Li, Y., Zhang, W., Niu, J.F., and Chen, Y.S. (2013). Surface-coating-dependent dissolution, aggregation, and reactive oxygen species (ROS) generation of silver nanoparticles under different irradiation conditions. Environ. Sci. Technol. *47*, 10293–10301. https://doi.org/10.1021/es400945v.

Lide, D.R. (2001). Handbook of Chemistry and Physic, 82nd ed. (CRC Press).

Liu, C., Leng, W., and Vikesland, P.J. (2018). Controlled evaluation of the impacts of surface coatings on silver nanoparticle dissolution rates. Environ. Sci. Technol. *52*, 2726–2734. https://doi.org/10.1021/acs.est.7b05622.

Liu, J., and Hurt, R.H. (2010). Ion release kinetics and particle persistence in aqueous nano-silver colloids. Environ. Sci. Technol. *44*, 2169–2175. https://doi.org/10.1021/es9035557.

Liu, M., Luo, G., Wang, Y., Xu, R., Wang, Y., He, W., Tan, J., Xing, M., and Wu, J. (2017). Nano-silver-decorated microfibrous eggshell membrane: processing, cytotoxicity assessment and optimization, antibacterial activity and wound healing. Sci. Rep. *7*, 436. https://doi.org/10.1038/s41598-017-00594-x.

Lofton, C., and Sigmund, W. (2005). Mechanisms controlling crystal habits of gold and silver colloids. Adv. Funct. Mater. *15*, 1197–1208. https://doi.org/10.1002/adfm.200400091.

Long, Y.M., Hu, L.G., Yan, X.T., Zhao, X.C., Zhou, Q.F., Cai, Y., and Jiang, G.B. (2017). Surface ligand controls silver ion release of nanosilver and its antibacterial activity against Escherichia coli. Int. J. Nanomed. *12*, 3193–3206. https://doi.org/10.2147/ijn.s132327.

Lu, D.W., Liu, Q., Zhang, T.Y., Cai, Y., Yin, Y.G., and Jiang, G.B. (2016). Stable silver isotope fractionation in the natural transformation process of silver nanoparticles. Nat. Nanotechnol. *11*, 682–686. https://doi.org/10.1038/nnano.2016.93.

Ma, R., Levard, C., Marinakos, S.M., Cheng, Y.W., Liu, J., Michel, F.M., Brown, G.E., and Lowry, G.V. (2012). Size-controlled dissolution of organic-coated silver nanoparticles. Environ. Sci. Technol. *46*, 752–759. https://doi.org/10.1021/es201686j.

Mitrano, D.M., Rimmele, E., Wichser, A., Erni, R., Height, M., and Nowack, B. (2014). Presence of nanoparticles in wash water from conventional silver and nano-silver textiles. ACS Nano *8*, 7208–7219. https://doi.org/10.1021/nn502228w.

Mittelman, A.M., Fortner, J.D., and Pennell, K.D. (2015). Effects of ultraviolet light on silver nanoparticle mobility and dissolution. Environmental Science-Nano *2*, 683–691. https://doi.org/10.1039/c5en00145e.

Molleman, B., and Hiemstra, T. (2015). Surface structure of silver nanoparticles as a model for understanding the oxidative dissolution of silver ions. Langmuir *31*, 13361–13372. https://doi.org/10.1021/acs.langmuir.5b03686.

Molleman, B., and Hiemstra, T. (2017). Time, pH, and size dependency of silver nanoparticle dissolution: the road to equilibrium. Environmental Science-Nano *4*, 1314–1327. https://doi.org/10.1039/c6en00564k.

Nowack, B. (2010). Nanosilver revisited downstream. Science *330*, 1054–1055. https://doi.org/10.1126/science.1198074.

Nowack, B., Krug, H.F., and Height, M. (2011). 120 Years of nanosilver history: implications for policy makers. Environ. Sci. Technol. *45*, 1177–1183. https://doi.org/10.1021/es103316q.

Park, J., Joo, J., Kwon, S.G., Jang, Y., and Hyeon, T. (2007). Synthesis of monodisperse spherical nanocrystals. Angew. Chem. Int. Ed. *46*, 4630–4660. https://doi.org/10.1002/anie.200603148.

Peng, M.W., Yu, X.L., Guan, Y., Liu, P., Yan, P., Fang, F., Guo, J., and Chen, Y.P. (2019). Underlying promotion mechanism of high concentration of silver nanoparticles on anammox process. ACS Nano *13*, 14500–14510. https://doi.org/10.1021/acsnano.9b08263.

Peretyazhko, T.S., Zhang, Q., and Colvin, V.L. (2014). Size-controlled dissolution of silver nanoparticles at neutral and acidic pH conditions: kinetics and size changes. Environ. Sci. Technol. *48*, 11954–11961. https://doi.org/10.1021/es5023202.

Pokhrel, L.R., Dubey, B., and Scheuerman, P.R. (2013). Impacts of select organic ligands on the colloidal stability, dissolution dynamics, and toxicity of silver nanoparticles. Environ. Sci. Technol. *47*, 12877–12885. https://doi.org/10.1021/es403462j.

Pokhrel, L.R., Dubey, B., and Scheuerman, P.R. (2014). Natural water chemistry (dissolved organic carbon, pH, and hardness) modulates colloidal stability, dissolution, and antimicrobial activity of citrate functionalized silver nanoparticles. Environmental Science-Nano *1*, 45–54. https://doi.org/10.1039/c3en00017f.

Pourzahedi, L., Vance, M., and Eckelman, M.J. (2017). Life cycle assessment and release studies for 15 nanosilver-enabled consumer products: investigating hotspots and patterns of contribution. Environ. Sci. Technol. *51*, 7148–7158. https://doi.org/10.1021/acs.est.6b05923.

Rizzello, L., and Pompa, P.P. (2014). Nanosilver-based antibacterial drugs and devices: mechanisms, methodological drawbacks, and guidelines. Chem. Soc. Rev. *43*, 1501–1518. https://doi.org/10.1039/c3cs60218d.

Rogers, K.R., Navratilova, J., Stefaniak, A., Bowers, L., Knepp, A.K., Al-Abed, S.R., Potter, P., Gitipour, A., Radwan, I., Nelson, C., and Bradham, K.D. (2018). Characterization of engineered nanoparticles in commercially available spray disinfectant products advertised to contain colloidal silver. Sci. Total Environ. *619–620*, 1375–1384. https://doi.org/10.1016/j.scitotenv.2017.11.195.

Rong, H.Y., Garg, S., and Waite, T.D. (2019). Impact of light and suwanee river fulvic acid on O-2 and H2O2 mediated oxidation of silver nanoparticles in simulated natural waters. Environ. Sci. Technol. *53*, 6688–6698. https://doi.org/10.1021/acs.est.8b07079.

Su, Y.M., Ashworth, V.E.T.M., Ashworth, V., Geitner, N.K., Wiesner, M.R., Ginnan, N., Rolshausen, P., Roper, C., and Jassby, D. (2020). Delivery, fate, and mobility of silver nanoparticles in citrus trees. ACS Nano *14*, 2966–2981. https://doi.org/10.1021/acsnano.9b07733.

Tortella, G.R., Rubilar, O., Durán, N., Diez, M.C., Martínez, M., Parada, J., and Seabra, A.B. (2020). Silver nanoparticles: toxicity in model organisms as an overview of its hazard for human health and the environment. J. Hazard Mater. *390*, 121974. https://doi.org/10.1016/j.jhazmat.2019.121974.

Tulve, N.S., Stefaniak, A.B., Vance, M.E., Rogers, K., Mwilu, S., LeBouf, R.F., Schwegler-Berry, D., Willis, R., Thomas, T.A., and Marr, L.C. (2015). Characterization of silver nanoparticles in selected consumer products and its relevance for predicting children's potential exposures. Int. J. Hyg Environ. Health *218*, 345–357. https://doi.org/10.1016/j.ijheh.2015.02.002.

Wang, D.S., Xie, T., Peng, Q., and Li, Y.D. (2008). Ag, Ag2S, and Ag2Se nanocrystals: synthesis, assembly, and construction of mesoporous structures. J. Am. Chem. Soc. *130*, 4016–4022. https://doi.org/10.1021/ja710004h.

Wei, L.Y., Lu, J.R., Xu, H.Z., Patel, A., Chen, Z.S., and Chen, G.F. (2015). Silver nanoparticles: synthesis, properties, and therapeutic applications. Drug Discov. Today *20*, 595–601. https://doi.org/10.1016/j.drudis.2014.11.014.

Xiu, Z.-M., Ma, J., and Alvarez, P.J.J. (2011). Differential effect of common ligands and molecular oxygen on antimicrobial activity of silver nanoparticles versus silver ions. Environmental Science & Technology *45*, 9003–9008. https://doi.org/10.1021/es201918f.

Xiu, Z.M., Zhang, Q.B., Puppala, H.L., Colvin, V.L., and Alvarez, P.J.J. (2012). Negligible particle-specific antibacterial activity of silver nanoparticles. Nano Lett. *12*, 4271–4275. https://doi.org/10.1021/nl301934w.

Yang, X.Y., Gondikas, A.P., Marinakos, S.M., Auffan, M., Liu, J., Hsu-Kim, H., and Meyer, J.N. (2012). Mechanism of silver nanoparticle toxicity is dependent on dissolved silver and surface coating in Caenorhabditis elegans. Environ. Sci. Technol. *46*, 1119–1127. https://doi.org/10.1021/es202417t.

Yang, Y., Zheng, S., Li, R., Chen, X., Wang, K., Sun, B., Zhang, Y., and Zhu, L. (2021). New insights into the facilitated dissolution and sulfidation of silver nanoparticles under simulated sunlight irradiation in aquatic environments by extracellular polymeric substances. Environ. Sci. J. Integr. Environ. Res.: Nano *8*, 748–757. https://doi.org/10.1039/d0en01142h.

Yuan, B.J., Sui, M.H., Lu, H.T., Wang, J.Y., and Qin, J. (2020). The combined effect of light irradiation and chloride on the physicochemical properties of silver nanoparticles. RSC Adv. *10*, 228–235. https://doi.org/10.1039/c9ra09261g.

Zhang, Q., Xie, J., Lee, J.Y., Zhang, J., and Boothroyd, C. (2008). Synthesis of Ag@AgAu metal core/alloy shell bimetallic nanoparticles with tunable shell compositions by a galvanic replacement reaction. Small *4*, 1067–1071. https://doi.org/10.1002/smll.200701196.

Zhang, Q., Xie, J., Yu, Y., and Lee, J.Y. (2010). Monodispersity control in the synthesis of monometallic and bimetallic quasi-spherical gold and silver nanoparticles. Nanoscale *2*, 1962. https://doi.org/10.1039/c0nr00155d.

Zhang, Q.B., Xie, J.P., Yang, J.H., and Lee, J.Y. (2009). Monodisperse icosahedral Ag, Au, and Pd nanoparticles: size control strategy and superlattice formation. ACS Nano *3*, 139–148. https://doi.org/10.1021/nn800531q.

Zhang, Q., Li, N., Goebl, J., Lu, Z.D., and Yin, Y.D. (2011a). A systematic study of the synthesis of silver nanoplates: is citrate a "magic" reagent? J. Am. Chem. Soc. *133*, 18931–18939. https://doi.org/10.1021/ja2080345.

Zhang, W., Yao, Y., Sullivan, N., and Chen, Y.S. (2011b). Modeling the primary size effects of citrate-coated silver nanoparticles on their ion release kinetics. Environ. Sci. Technol. *45*, 4422–4428. https://doi.org/10.1021/es104205a.

STAR★METHODS

KEY RESOURCES TABLE

REAGENT or RESOURCE	SOURCE	IDENTIFIER
Bacterial and virus strains		
E. coli strain K12	ATCC	ATCC 25404
Chemicals, peptides, and recombinant proteins		
Silver perchlorate (anhydrous, 97%)	Sigma-Aldrich	Cat#674583
Silver nitrate (>99%)	Sigma-Aldrich	Cat#S8157
Oleic acid (technical grade, 90%)	Sigma-Aldrich	Cat#364525
1,2-hexadecanediol (technical grade, 90%)	Sigma-Aldrich	Cat#213748
4-tert-butyltoluene (>95%)	Sigma-Aldrich	Cat#B102628
Oleylamine (technical grade, 70%)	Sigma-Aldrich	Cat#O7805
Octadecylamine (>97%)	Sigma-Aldrich	Cat#305391
Tri-sodium citrate dihydrate (>99%)	Sigma-Aldrich	Cat#W302600
Sodium borohydride (*ReagentPlus*, 99%)	Sigma-Aldrich	Cat#109169
Poly(vinyl alcohol) (PVA, MW = 9,000–10,000)	Sigma-Aldrich	Cat#360627
Polyvinylpyrrolidone (PVP, MW = 10,000)	Sigma-Aldrich	Cat#PVP10
Yeast extract	Sigma-Aldrich	Cat#Y1625
Potassium oleate (technical grade, >98%)	Fisher Scientific	Cat#O005625G
Sodium bicarbonate (99.9%)	Fisher Scientific	Cat#AAJ65594A1
Hydrogen peroxide aqueous solution (30%)	Fisher Scientific	Cat#H325-500
Poly (ethylene glycol) thiol (1k)	Creative PEGWorks	Cat#PJK-606
Poly (ethylene glycol) thiol (2k)	Creative PEGWorks	Cat#PJK-605
Poly (ethylene glycol) thiol (5k)	Creative PEGWorks	Cat#PJK-604
Poly (ethylene glycol) thiol (10k)	Creative PEGWorks	Cat#PJK-603
Poly (ethylene glycol) thiol (20k)	Creative PEGWorks	Cat#PJK-602
Poly (ethylene glycol) thiol (30k)	Creative PEGWorks	Cat#PJK-601
Software and algorithms		
Sigma-Plot 11.0	Systat Software Inc	https://systatsoftware.com/

RESOURCE AVAILABILITY

Lead contact

Further information and requests for resources and reagents should be directed to and will be fulfilled by the lead contact, Vicki L. Colvin (vicki_colvin@brown.edu).

Materials availability

This study did not generate new unique reagents.

Data and code availability

- All data reported in this paper will be shared by the lead contact upon request.
- This paper does not report original code.
- Any additional information required to reanalyze the data reported in this paper is available from the lead contact upon request.

EXPERIMENTAL MODEL AND SUBJECT DETAILS

Bacteria

E. coli strain K12 (ATCC 25404) was used as a model microorganism to evaluate the antibacterial activity of the silver nanoparticles. The cells were grown in LB (Luria-Bertani) media.

METHOD DETAILS

Silver nanoparticles with different size

Silver nanoparticles with different size were synthesized in the organic solvent and then transferred into water using PEG-SH. The high boiling point of the organic solvent allows for the synthesis of nanoparticles at high temperature, which favors burst nucleation and diffusion-controlled growth, leading to highly monodisperse nanoparticles (Park et al., 2007). The size of the nanoparticles were controlled by the nature of the precursor, reducing agent, and capping agent, combined with the concentration of the reactants and temperature (Zhang et al., 2010).

Silver nanoparticles of 2.9 nm diameter were synthesized by reducing silver oleate with oleylamine following a modified version of an existing procedure(Li et al., 2011). Silver oleate was prepared by mixing 850. mg of $AgNO_3$ (Sigma-Aldrich, >99%), 1605. mg of potassium oleate (Fisher, 98%), 25. mL of ethanol (Sigma, 99%), 34. mL of deionized water, and 67. mL of hexanes (Fisher, 98.5%) in a round-bottom flask. The mixture was heated to 45°C and held at that temperature for five hours, forming a white solid product of silver oleate. The solid product was collected and washed with water and ethanol six times and then dried in vacuum. Next, 540. mg of as-synthesized silver oleate, 6.8 mL of oleic acid (Sigma, 99%) and 8.3 mL of dodecylamine (Sigma, >99%) were mixed in a round-bottom flask connected to a Schlenk line; oxygen in the air above the solution was removed via three consecutive nitrogen purges followed by vacuum ($\sim 10^{-3}$ atm). The solution was then heated to 155°C for 1 h, during which time the color changed from a clear yellow solution to a deep brown solution. After cooling the solution, roughly 30 mL of acetone (Fisher, 99.5%) were added to the solution and the particles were collected by centrifugation (9000 rpm, 10 min). The nanoparticle residue was further treated with four centrifugation and redispersion cycles using 5 mL of hexane and 35 mL of acetone to remove unreacted reactants, solvent, and byproducts. The purified silver nanoparticles were ultimately suspended in hexanes (Fisher, 98.5%) and stored in a foil wrapped vial under nitrogen until aqueous phase transfer.

To synthesize 4.7 nm diameter silver nanoparticles, 698. mg of silver perchlorate (Sigma, 97%), 45 mL of octadecene (Sigma, 90%), and 6 mL of oleic acid (Sigma 99%) were mixed in a round-bottom flask connected to a Schlenk line. The vessel was purged with nitrogen and vacuum ($\sim 10^{-3}$ atm) three times to remove oxygen, and then heated to 70°C for 45 min, at which point it was a clear and colorless solution. At this point, 0.36 mL of oleylamine (Sigma, 70%) was quickly injected into the solution whereupon a yellow color was observed. This reaction mixture was then heated to 150°C and held for four hours, after which the solution formed a dark brown color. The nanoparticles were recovered, purified and stored in hexanes (Fisher, 98.5%) following the procedure outlined for the 2.9 nm diameter materials.

Silver nanoparticles of 9.1 nm were synthesized using a modified procedure in literature (Zhang et al., 2009). Briefly, 510. mg of 1,2-hexadecanediol (Sigma, 90%) was added to 17 mL of 4-tert-butyltoluene (Sigma, 95%) in a round bottom flask and the mixture was heated to 191°C at which time it was a colorless clear solution. To initiate the formation of silver nanocrystals, another solution containing 170. mg of $AgNO_3$ (Sigma, 99%), 1.7 mL of oleylamine (Sigma, 70%), and 10 mL of 4-tert-butyltoluene (Sigma, 95%) was injected quickly into the starting 1,2-hexadecanediol solution while vigorously stirring the solution. This dark brown mixture was refluxed for 4 min at 191°C and then allowed to cool down after removing the heating mantle. At this stage, very small silver nanoparticles have formed and these were precipitated by adding ethanol (Sigma, 99%) to the solution and washed with ethanol to remove the impurities. These purified silver nanoparticles were then combined with 3.5 mL of dodecylamine (Sigma, >99%), and 32 mL of 4-tert-butyltoluene (Sigma, 95%) in a round-bottom flask connected to a Schlenk line. To remove oxygen, the solution was subjected to three consecutive nitrogen purge and vacuum ($\sim 10^{-3}$ atm) treatments, after which time it was refluxed for 36 h at 192°C. The silver nanoparticles were precipitated by ethanol and then redispersed in 4-tert-butyltoluene (Sigma, 95%) for further seeded growth. Alternatively they were recovered, purified and stored in hexanes as described previously.

Silver nanoparticles of 13.0 and 17.3 nm diameter were synthesized through a seeded growth method by using 9.1 nm diameter silver nanoparticles as seeds (Zhang et al., 2009). First, 100. mg of 1,2-hexadecanediol (Sigma, 90%) was added to 10. mL 4-tert-butyl toluene (Sigma, 95%) and the mixture was heated to 130°C. Next, 1.0 mL of a 10 mM silver nanoparticle seed solution was added, followed by addition of 2.0 mL or 6.0 mL of a 10 mM $AgNO_3$ (Sigma, 99%) solution prepared in 4-tert-butyltoluene (Sigma, 95%). This addition was done in a dropwise fashion to yield Ag nanoparticles with different diameters, after which time the solution remained at 130°C for 15 min in order to completely reduce the silver ions. The as-synthesized silver nanoparticles were first precipitated and washed by 40 mL of ethanol (Sigma, 99%). Following this, the nanoparticles were recovered, purified and stored in hexanes according to the procedure outlined for the 2.9 nm diameter materials.

Phase transfer of silver nanoparticles

The silver nanoparticles were transferred from hexanes to water using PEG-SH (Krueger et al., 2007). The phase transfer was carried out under nitrogen. A 0.2 mL solution of silver nanoparticles in hexanes (~400 mg Ag/L) was mixed with 20. mL diethyl ether (Sigma, 99%) under magnetic stirring. 0.04 mL of a chloroform (Sigma, 99%) solution of poly(ethylene glycol) thiol (5 kDa, 10 mg/mL, Creative) was added to the silver nanoparticle solution slowly over 1 min. Next, 20. mL of deoxygenated water was added to the solution. After about five minutes, the color of the top organic solution became clear and the bottom aqueous phase became brownish yellow, indicating the successful transfer of silver nanoparticles into water. Silver nanoparticles in aqueous solution were then purified with deoxygenated water using an Amicon ultrafiltration stirred cell (EMD, UFSC05001) to remove the impurities. Briefly, the silver nanoparticle solution was transferred to a stirred cell equipped with a Bioma ultrafiltration membrane with molecular weight cut-off of 100 kDa (EMD, PBHK04310). The stirred cell was connected with a stirred cell reservoir (EMD, #6028) and compressed nitrogen through a selector valve (EMD, # 6003). By switching the selector valve, the stirred cell was either directly connected to the compressed nitrogen or connected to the water reservoir. When the stirred cell was connected to the compressed nitrogen, the compressed nitrogen served as the pressure source to filter the silver nanoparticle solution. When the stirred cell was connected to the reservoir, the compressed nitrogen pressed the water in the reservoir into the stirred cell. The products were washed more than six times by switching the selector valve.

Silver nanoparticles with different shapes

Both the silver nanoplates and nanospheres were produced using a two-step seeded growth procedure to make sure the two types of nanoparticles have the same surface coating and similar volume. Citrate was used as capping agent throughout the two steps for synthesis of both nanoplates and nanospheres to ensure identical surface chemistry. In the first step, small silver nanoplates and nanospheres were generated by reduction of silver ions in aqueous solution. In the second step, these small nanoplates and nanopspheres were used as seeds to prepare larger nanoplates and nanospheres. The size of the nanoparticles can be controlled by the ratio of the seeds and precursor added. Generation of silver nanoparticles in two separate steps allows for the independent control of nanoparticle shape and size, which makes it possible to produce silver nanoplates and nanospheres with similar volume.

Big silver nanospheres were synthesized from small nanospheres as seeds (Zhang et al., 2008). First, small silver nanosphere seeds were synthesized by reducing silver nitrate with $NaBH_4$ (Sigma, 99%). Next, 1.6 mL of 40 mM aqueous solution of tri-sodium citrate (Sigma, 99%) solution and 1.0 mL of 20 mM solution of silver nitrate (Sigma, 99%) were added to 17.0 mL deionized H_2O (18.2 MΩ). Then, 0.4 mL of 100 mM ice-cold aqueous $NaBH_4$ (Sigma, 99%) solution was added dropwise under vigorous stirring. The color of the reaction solution changed to yellow immediately upon of the addition of $NaBH_4$ solution, indicating the formation of silver nanospheres. The aqueous solution of silver nanoparticles was aged for 24 h to ensure that there was no residual $NaBH_4$. These small Ag nanospheres were used as seeds to obtain larger Ag nanospheres. In order to generate big silver nanospheres, 58. mL of 18. mM aqueous sodium citrate (Sigma, 99%) solution was heated to the boiling point, and 1 mL of the as-synthesized silver nanoparticle seeds solution was added, after which 158. mL of a 1.36 mM aqueous solution of $AgNO_3$ (Sigma, 99%) was added slowly to the solution over 10 min, and the mixture was refluxed for 30 more minutes. After cooling, the silver nanospheres were purified using stirred cell to remove unreacted reactants and byproducts. The diameter of silver nanoparticles obtained from this procedure is 45.4 $\pm$ 5.4 nm.

Silver nanoplates were also synthesized using the two-step seeded growth method (Li et al., 2012). First, small Ag nanoplates were prepared by modifying an existing procedure (Zhang et al., 2011a). Briefly, 0.165 mL of 5 mM $AgNO_3$ (Sigma, 99%) solution, 0.425 mL of 30 mM tri-sodium citrate (Sigma, 99%) solution, and 0.1 mL of H_2O_2 (Fisher, 6 wt %) were mixed with 7.83 mL water under vigorously stirring. Next, 88 μL of 0.1 M $NaBH_4$ (Sigma, 99%) solution was quickly injected into this mixture, and the mixture solution was stirred vigorously for 30 more minutes. The solution was aged for 12 h to fully react any sodium borohydride. Next, the as-synthesized small nanoplates were used as seeds to prepare larger nanoplates. For this step, 8. mL of silver nanoplates seed solution, 8. mL of 30 mM sodium citrate solution, 4. mL of 0.2 M ascorbic acid (Sigma, 99%) solution were mixed with 32 mL H_2O in a beaker. Then, 10.5 mL of 0.5 mM $AgNO_3$ (Sigma, 99%) solution was added dropwise to the solution over 3 min. The mixture was stirred for 10 more minutes, and the resulting silver nanoplates were purified with a stirred cell to remove unreacted reactants and byproducts. The absorption spectrum of the as-synthesized nanoprims shows three peaks at around 330 nm, 688 nm and 1038 nm, corresponding to the in-plane dipolar, in-plane quardrupole, and out-of-plane quadrupole resonances, respectively.

Silver nanoparticles with different coatings

Silver nanoparticles coated with citrate were synthesized using a seeded growth method similar to the procedure detailed for producing 45.4 nm diameter silver nanospheres. The process begins with the same seed solution as described for the nanosphere product. First, 1.0 mL of the silver nanoparticle seed solution was added to 28. mL of a boiling sodium citrate solution (6 mM). Next, 7.0 mL of 5. mM $AgNO_3$ solution was added to the solution dropwise over 5 min, and the mixture was refluxed for 30 more minutes. The silver nanoparticles were purified with stirred cell to remove all the impurities. The diameter of silver nanoparticles obtained from this process was 23.5 $\pm$ 2.6 nm. The silver nanoparticles of this size was also used for the study of the concentration-dependent dissolution.

Silver nanoparticles coated with polyvinylpyrrolidone, poly (vinyl alcohol), and poly(ethylene glycol) thiol were prepared through ligand exchange from the as-synthesized silver nanoparticles coated with citrate. Briefly, 1 mL of aqueous solution of polymer (10 g/L polyvinylpyrrolidone (Sigma, 10,000), 2 g/L poly (vinyl alcohol) (Sigma, 9,000–10,000), 1 g/L poly(ethylene glycol) thiol (Creative, 10,000) were added to 10 mL of aqueous solution of silver nanoparticles coated with citrate under vigorous stirring. The mixture was stirred for 1 h at room temperature to replace citrate on the particles surface with polymer. The silver nanoparticles were purified with a stirred cell to remove the free ligands and other impurities. The process was repeated twice to ensure complete ligand exchange.

Silver nanoparticles with different PEG length

The initial silver nanoparticles were synthesized according to a modified procedure reported in the literature (Wang et al., 2008). First, 10. mL of octadecylamine (Sigma, 97%) was heated to 180°C in a round bottom flask, to which 0.5 g of $AgNO_3$ solid (Sigma, 99%) was added quickly under vigorous stirring. The mixture was maintained at 180°C for 35 min and then cooled down to 65 °C. Next, 50. mL of hexanes (Fisher, 98.5%) and 2. mL of oleic acid (Sigma, 99%) was added to the reaction mixture and maintained at this temperature for 30 more minutes before cooling down. The silver nanoparticles formed were precipitated using acetone and purified using acetone and hexanes. The purified silver nanoparticles were redispersed in hexanes for phase transfer. Poly(ethylene glycol) thiol (PEG-SH) with molecular weights of 1,000, 2,000, 5,000, 10,000, 20,000, and 30,000 Da (Creative PEGworks) were used to transfer silver nanoparticles to water; the manufacturer specifies the PDI of 1.08, 1.08, 1.06, 1.02, 1.04, and 1.05 for PEG-SH with molecular weights of 1,000, 2,000, 5,000, 10,000, 20,000, and 30,000, respectively. The weight ratio of silver to PEG-SH with different molecular weights were 1:1, 1:1.5, 1:2.5, 1:5, 1:10, 1:15, respectively.

Transmission electron microscopy

Transmission electron microscopy (TEM) images were acquired by a JEOL 2100 field emission gun TEM (FEG-TEM). The FEG-TEM was operated at 200 keV with a single sample holder. Samples were prepared by the evaporation of ~3 uL of a dispersed solution of silver nanoparticles on a carbon type-A 400 mesh copper grid (Ted Pella). The diameter distribution of silver nanoparticles was obtained by counting more than 1,500 particles using the software of Image-Pro Plus 5.0.

Infrared spectroscopy

The surface coatings of silver nanoparticles were determined by Fourier Transform Infrared (FT-IR) spectroscopy. The FT-IR spectra of the samples were measured using a Fourier Transform Infrared spectrometer (Nicolet iS50) in transmission mode.

Optical spectroscopy

The UV-Vis absorbance spectra of silver nanoparticles solution were obtained using a UV-vis-NIR spectrophotometer (Cary 5000, Varian). Silver nanoparticles in organic solvents were measured using quartz cuvettes with 10 mm path length. Aqueous samples were measured in disposable polystyrene cuvettes with 10 mm path length.

Atomic emission spectroscopy

The total concentration of silver in the solution was measured using a inductively coupled plasma atomic emission spectroscope (ICP-AES) equipped with an auto sampler (Perkin-Elmer). The samples were prepared by digestion of silver nanoparticles using HNO_3 (Sigma, 70%) and H_2O_2 (Fisher, 30%). Briefly, 0.4 mL of silver nanoparticle sample was mixed with 1.5 mL of HNO_3 and heated at 70°C for about 1 h before cooling down. The sample was then treated with 1 mL of H_2O_2 for 1 more hour. The resulting solution was then transferred to a 50 mL volumetric flask and diluted to 50 mL using DI-water (Millipore, 18.2 MΩ).

Dynamic light scattering

The hydrodynamic diameter of the silver nanoparticles was measured using a Malvern ZEN-3600 Zetasizer Equipped with a HeNe 633 nm laser (Malvern, UK) at 25°C. The average size was obtained over three measurements for each sample.

X-ray photoelectron spectroscopy

X-ray photoelectron spectroscopic (XPS) data was collected using a PHI Quantera XPS with a monochromatic aluminum 38.6 W X-ray source and 200.0 μm X-ray spot size with a pass energy of 26.00 eV at 45.0°. The silver nanoparticles wer collected by centrifuge and dried in vacuum before XPS measurement.

Measurement of PEG grafting density

The grafting density of PEG on nanoparticle surfaces was determined following a method in the literature (Benoit et al., 2012). Organic carbon concentrations were measured using Shimadzu TOC-VWP total organic carbon (TOC) analyzer with auto sampler. The samples were run on a total nonpurgeable organic carbon assay with triplicate 50 μL injection volumes. The grafting density (σ) of PEG on silver nanoparticle surfaces was calculated using the following:

$$\sigma = \frac{[C]}{2n[NP]2\Pi r^2}$$

where [C] is the molar concentration of carbon determined from TOC, n is the number of monomers in each polymer sample, [NP] is the molar concentration of silver nanoparticles calculated from the concentration of silver determined from ICP and the diameter of the nanoparticles determined from TEM, and r is the radius of the nanoparticles determined from TEM.

Measurement of silver dissolution

The dissolution properties of silver nanoparticles were determined by monitoring the concentration of silver ions released from the oxidative dissolution of silver nanoparticles with time. The concentration of silver ions was measured using a silver/sulfide ion selective electrode (Cole-Parmer, EW-27504-28) according to the method in the literature (Peretyazhko et al., 2014; Tulve et al., 2015). The ion selective electrode only detects silver in the form of free ions and is not influenced by silver nanoparticles, thus allowing direct measurement of the concentration of silver ions without separation from nanoparticles. The silver nanoparticle solution was diluted to 12 mg/L right after the purification, and 10. mL of silver nanoparticle aqueous solution was transferred to a 20 mL transparent scintillation glass vial. The vials were then placed on the bench under ambient atmospheric and room light, and the evolution of free silver ions over time was measured. The electrode was calibrated prior to use at the beginning of each experiment.

The measured data was fitted using the first-order reaction model as described in the following Equation 2 (Peretyazhko et al., 2014; Zhang et al., 2011b).

$$[Ag^+]_{(t)} = [Ag^+]_{eq}\left(1 - e^{-kt}\right)$$

Where $[Ag^+]_{eq}$ is the equilibrium concentration of silver ions, $[Ag^+]_{(t)}$ is the silver ion concentration at time (t), k is the rate constant, respectively.

Measurement of the antibacterial activity

E. coli strain K12 (ATCC 25404) was used as a model microorganism to evaluate the antibacterial activity of the silver nanoparticles following the procedure in the literature (Xiu et al., 2011, 2012). A single colony of *E. coli* grown on LB agar plates was inoculated in 50 mL of LB Broth and grown in a shaking incubator at 37°C for 6 h. The bacteria were harvested and washed three times with 2 mM sodium bicarbonate buffer solution. The bacteria were then resuspended in 2mM sodium bicarbonate buffer solution at the viable cell concentration of $\sim 1.8 \times 10^8$ cells/mL.

The dose-response relationships were determined by measuring the mortality of *E. coli* in silver nanoparticle solutions with different concentrations. For each silver nanoparticle sample, a series of silver nanoparticle solutions with different concentrations were prepared. The concentration of the sodium bicarbonate in these solutions was 2 mM. Briefly, 0.18 mL of the silver nanoparticle solution was mixed with 0.02 mL of bacteria solution in a 96 well plate. The mixture was incubated in the dark for 20 h at 23°C under anaerobic environment. *E. coli* mortality in different treatments was then determined by viable plate counts and calculated as $1\text{-}N/N_0 \times 100\%$, where N and N_0 are the remaining and initial concentrations of viable bacteria (CFU/mL), respectively.

EC_{50}, silver concentration that results in 50% mortality, was estimated from the dose-response relationships of *E. coli* mortality versus silver concentrations. The dose-response relationships were fitted according to the the following equation using the software of Sigma-Plot (v11.0):

$$y = y_0 + \frac{a}{1 + e^{-\frac{x - x_0}{b}}}$$

where y is the *E. coli* mortality rate, y_0 is the baseline mortality rate without silver addition, x is silver concentration, and x_0 is EC_{50}. All tests were conducted in triplicate.

QUANTIFICATION AND STATISTICAL ANALYSIS

Quantification was performed as described in the relevant method details sections above. All data were presented as mean ± SD.